Semiclassical Calculations of Tunneling Splitting in Tropolone

Yin Guo,[†] Thomas D. Sewell,[‡] and Donald L. Thompson*[,†]

Department of Chemistry, Oklahoma State University, Stillwater, Oklahoma 74078, and Theoretical Division, Los Alamos National Laboratory, Los Alamos, New Mexico 87545

Received: December 5, 1997; In Final Form: April 10, 1998

Energy level splittings in tropolone are calculated by using a semiclassical approach for tunneling in multidimensional systems. A potential-energy surface that includes all 39 vibrational degrees of freedom was constructed for the ground electronic state on the basis of ab initio results. Since the method incorporates tunneling within standard trajectory simulations, the full-dimensional dynamics were explicitly treated to provide a clear picture of the dynamical behavior of the system and its effect on tunneling. Level splittings for the ground states of the normal and deuterated species were calculated. We also studied the sensitivity of the splittings to the choice of tunneling path. Mode-selective excitations were used to study the effect of vibrational excitation on the tunneling. It is found that some modes promote tunneling, some suppress it, and some do not affect it. This demonstrates the multidimensional nature of the tunneling process and the importance of properly treating heavy-atom motions.

1. Introduction

This is a continuation of a series of studies[1−7] of tunneling effects in multidimensional sytems by using semiclassical methods that incorporate tunneling into standard classical trajectory simulations. The approach is practical for large systems where full quantum-mechanical solutions are not feasible. It also provides clear insight into the dynamical nature of the tunneling effects since the full-dimensional classical dynamics are explicitly treated. The basic idea is that classical trajectories are initiated in the usual quasiclassical way and propagated in the classically allowed regions of phase space, with tunneling probabilities computed at turning points along some predefined tunneling direction. The rate coefficient or energy level splitting is calculated by averaging over an ensemble of trajectories corresponding to a specified quantum state.

Our recent study of the collinear H + H_2 atom-exchange reaction shows that this simple approach is quite accurate for small systems.[7] The calculated H + H_2 reaction probabilities are in good agreement with the quantum-mechanical values and are in fact as good as the results obtained from more sophisticated semiclassical methods such as **S**-matrix theory[8] and the instanton model.[9] For large systems, where quantum mechanical calculations are not feasible and thus semiclassical methods are most useful, comparisons can only be made with experimental data. Calculations of the ground-state splittings in several isotopomers of malonaldehyde[4] and methylmalonaldehyde,[6] for which all the vibrational degrees of freedom were included, indicate that the method may be accurate in many-atom systems as well. The computed splittings agree with the experimental values to within a factor of 2.

The main purpose of this study is to further investigate and test this semiclassical approach. The isomerization of tropolone (see Figure 1) presents an interesting case because of the availability of a large body of experimental data.[10−19] In addition to the vibrational ground-state splittings in the ground and first-excited electronic states (X and $\tilde{A}$), some splittings of vibrationally excited states have been measured for the $\tilde{A}$ state. The most interesting (but not surprising) finding is that tunneling strongly depends on the level of the excitation and the character of the mode; some modes promote tunneling, some suppress it, and some do not affect it. This clearly demonstrates the effects of multidimensional dynamics on the hydrogen-atom transfer process and in particular the importance of properly treating the heavy-atom motions. There are already a number of theoretical studies of tunneling in tropolone,[20−24] none of which

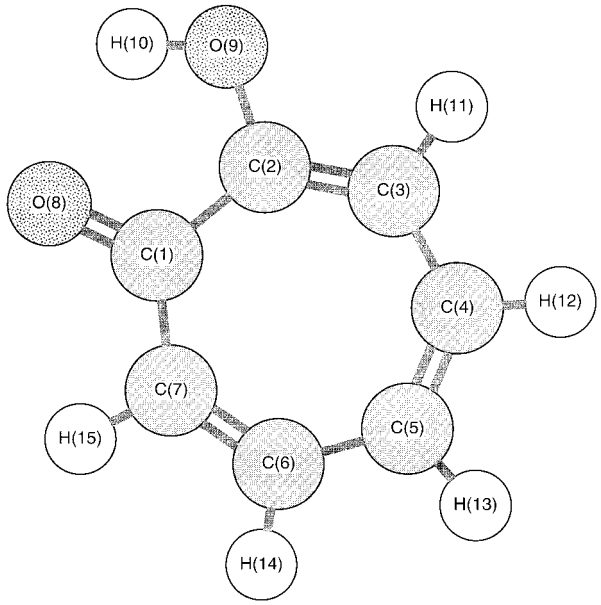

Figure 1. Schematic illustration of tropolone molecular structure and the atom-numbering scheme used in this work.

[†] Oklahoma State University.
[‡] Los Alamos National Laboratory.

S1089-5639(98)00445-9 CCC: $15.00
Published on Web 06/05/1998

explicitly treat the full-dimensional dynamics. Since our semiclassical approach allows for explicit treatment of the full-dimensional classical dynamics, it should provide greater insight into the tunneling mechanism in tropolone.

The observed tunneling splittings of the vibrationally excited levels are for the $\tilde{A}$ state. However, it is difficult to perform reliable ab initio calculations for an electronically excited state. We therefore constructed a potential-energy surface for the X state on the basis of ab initio calculations and used it in the tunneling calculations. Since it is reasonable to expect that many of the modes that significantly affect tunneling are similar for the X and $\tilde{A}$ states, the experimental data for the $\tilde{A}$ state of tropolone may be qualitatively interpreted from theoretical calculations for the X state.

2. Computational Methods

A. Potential-Energy Surface. The potential-energy surface used in this study is based on the results of ab initio calculations. The GAUSSIAN 92 programs were used to compute the geometries and energies of the equilibrium and transition-state structures for the ground electronic state at the MP2/6-31G** level. Normal-mode analyses were performed to verify the curvature at these stationary points, and frequencies for several additional isotopomers were computed and used in fitting the force field parameters. The calculated equilibrium structure is shown in Figure 1, and the values of the internal coordinates are given in Table 1.

Our goal is to treat the symmetric double-well tunneling dynamics of tropolone. Thus, the required potential-energy surface must describe the forces for geometries far removed from equilibrium, at least along the reaction coordinate for tautomerization. Moreover, the potential-energy surface must be symmetric with respect to hydrogen transfer and realistically describe the barrier to that process. To do this, we write the potential-energy surface as

$$V = S_1(R)V_A + [1 - S_1(R)]V_B \quad (1)$$

where V_A and V_B are the equilibrium force field potentials corresponding to the two symmetric isomers, expressed in terms of valence internal coordinates, and $S_1(R)$ is a switching function,

$$S_1(R) = {}^1/_2\{1 - \tanh[a(r_{OH} - r_{O\cdots H})]\} \quad (2)$$

that smoothly varies from zero to unity as a function of the reaction coordinate $R = r_{OH} - r_{O\cdots H}$, i.e., the difference between the two OH bond lengths. The purpose of $S_1(R)$ is to continuously vary the contributions of V_A and V_B to the potential energy depending on whether the system is near the equilibrium geometry of well A ($S_1(R) \rightarrow 1$), that of well B ($S_1(R) \rightarrow 0$), or somewhere between ($S_1(R) \rightarrow {}^1/_2$; i.e., transition statelike configurations).

The potentials V_A and V_B are written as a sum of Morse functions for the bond stretches, harmonic oscillators for the in-plane angle-bending and out-of-plane wag angle-bending terms, six-term cosine series for the dihedral angles, and harmonic bond−bond, angle−angle, and bond−angle interaction terms:

$$V_n = \sum_{i=1}^{16}\{D_{e,i}\exp[-2S_2(R)\alpha_i(r_i - r_i^0)] - 2D_{e,i}\exp[-S_2(R)\alpha_i(r_i - r_i^0)]\} + {}^1/_2\sum_{i=1}^{24}S_2(R)k_i(\theta_i - \theta_i^0)^2 + {}^1/_2\sum_{i=1}^{7}k_i(\gamma_i - \gamma_i^0)^2 + \sum_{i=1}^{11}\sum_{j=0}^{5}a_{ij}\cos(j(\tau_i - \tau_i^0)) + \sum_{i,j=1}^{9}k_{ij}^{\,a}(r_i - r_i^0)(r_j - r_j^0) + \sum_{i,j=1}^{9}k_{ij}^{\,b}(\theta_i - \theta_i^0)(\theta_j - \theta_j^0) + \sum_{i,j=1}^{20}k_{ij}^{\,c}(r_i - r_i^0)(\theta_j - \theta_j^0), \quad n = \text{A, B} \quad (3)$$

A second switching function $S_2(R)$ is used to adjust the width and height of the barrier to hydrogen transfer. It acts on the force constants for the harmonic in-plane bending potentials and on the Morse curvature parameter, α, for the O−H and O···H bonds. The form of $S_2(R)$ is

$$S_2(R) = 1 - b\exp(-cR^4) \quad (4)$$

where R is defined above. The values of the parameters in the switching functions were taken to be $a = 3.5$ Å^{-1}, $b = 0.28$, and $c = 25.0$ Å^{-4}.

Cross-terms can give rise to spurious minima in a potential-energy surface for geometries far from equilibrium and could potentially present a problem here due to the sizable zero-point energy of tropolone (~73 kcal/mol). However, we found no evidence of problems in the dynamics calculations considered in this work.

The values of the force field parameters were determined by adjusting them to minimize the sum of the squares of the differences between the values of the frequencies calculated using eq 1 and the ab initio values. The ab initio values were not scaled. The parent compound plus two additional isotopomers were considered in the fitting of the equilibrium force field to the ab initio results. The switching function parameters were adjusted to yield the desired barrier subject to the constraint that the switching functions have negligible effect at the equilibrium geometries. The values of the force field parameters are given in Table 1.

Equilibrium normal-mode frequencies for each of the three species used in fitting the force field are compared to the ab initio results in Table 2. Results for two additional isotopomers that were not used in determining the force field are given in Table 3. A satisfactory fit was obtained for all cases, including those that were not explicitly considered in the parametrization of the force field.

The barrier to H-atom transfer in the X state of tropolone is not known from experimental measurements. However, there are a number of calculations of it. The values range from 2.9 to 15.7 kcal/mol, depending on the level of theory.[24] Given this uncertainty, we have taken the pragmatic approach of arbitrarily adjusting the barrier height to yield a ground-state eigenvalue splitting in agreement with the experimental result for the parent compound and then using that barrier in subsequent calculations of the ground-state splitting for partially deuterated tropolone and for various mode-selective excitations. These latter results are then compared, insofar as is possible, to experimental data in order to assess the accuracy of the potential-energy surface and semiclassical approach. The classical barrier height is taken to be 16.0 kcal/mol in all of the calculations. This is near the value obtained at the HF/6-31G** level (15.7 kcal/mol)[24] and

TABLE 1: Potential-Energy Surface Parameters

Equilibrium Bond Lengths and Morse Potential Parameters

bond[a]	r^0 (Å)	α (Å^{-1})	D_e (kcal/mol)	bond[a]	r^0 (Å)	α (Å^{-1})	D_e (kcal/mol)
C_1-C_2	1.472 527	2.161 93	84.0	C_2-O_9	1.339 555	2.548 67	87.0
$C_2=C_3$	1.382 982	1.925 12	146.0	O_9-H_{10}	0.991 455	2.264 70	90.0
C_3-C_4	1.406 940	2.241 68	84.0	C_3-H_{11}	1.083 782	1.918 36	112.0
$C_4=C_5$	1.381 980	2.039 98	146.0	C_4-H_{12}	1.084 236	1.899 33	112.0
C_5-C_6	1.413 074	2.140 21	84.0	C_5-H_{13}	1.083 191	1.931 30	112.0
$C_6=C_7$	1.376 725	2.114 93	146.0	C_6-H_{14}	1.084 893	1.918 50	112.0
C_1-C_7	1.437 269	2.374 92	84.0	C_7-H_{15}	1.084 011	1.921 72	112.0
$C_1=O_8$	1.260 559	1.827 46	193.0	$O_8\cdots H_{10}$	1.791 032	1.004 07	10.0

Equilibrium Bend Angles and Harmonic Bending Force Constants

angle	θ^0 (deg)	k (kcal mol^{-1} rad^{-2})	angle	θ^0 (deg)	k (kcal mol^{-1} rad^{-2})	angle	θ^0 (deg)	k (kcal mol^{-1} rad^{-2})
$C_1C_2C_3$	130.3182	70.617	$H_{12}C_4C_5$	115.9190	79.387	$C_6C_7H_{15}$	117.2418	73.760
$C_1C_2O_9$	111.4789	67.418	$C_4C_5C_6$	127.7453	136.709	$H_{15}C_7C_1$	112.2990	76.698
$O_9C_2C_3$	118.2029	217.540	$C_4C_5H_{13}$	116.3195	94.951	$C_7C_1C_2$	123.2725	47.543
$C_2C_3C_4$	128.9406	152.684	$H_{13}C_5C_6$	115.9352	77.102	$C_7C_1O_8$	121.6887	278.186
$C_2C_3H_{11}$	114.0098	88.797	$C_5C_6C_7$	130.1077	119.638	$O_8C_1C_2$	115.0388	91.651
$H_{11}C_3C_4$	117.0496	75.439	$C_5C_6H_{14}$	115.0853	97.194	$C_2O_9H_{10}$	101.9229	61.524
$C_3C_4C_5$	129.1564	194.822	$H_{14}C_6C_7$	114.8069	77.963	$O_9H_{10}O_8$	125.3106	52.315
$C_3C_4H_{12}$	114.9246	76.049	$C_6C_7C_1$	130.4592	148.872	$C_1O_8H_{10}$	86.2489	33.662

Wag Angle Bending Interactions

wag angle	γ^0 (deg)	k_γ (kcal mol^{-1} rad^{-2})	wag angle	γ^0 (deg)	k_γ (kcal mol^{-1} rad^{-2})	wag angle	γ^0 (deg)	k_γ (kcal mol^{-1} rad^{-2})
$C_7C_1C_2O_8$	0.0	9.341	$C_3C_4C_5H_{12}$	0.0	8.435	$C_5C_6C_7H_{14}$	0.0	10.662
$C_1C_2C_3O_9$	0.0	80.032	$C_4C_5C_6H_{13}$	0.0	3.573	$C_6C_7C_1H_{15}$	0.0	25.229
$C_2C_3C_4H_{11}$	0.0	1.075						

Dihedral Angle Interactions (kcal/mol)

dihedral angle	τ^0 (deg)	a_0	a_2	a_4	dihedral angle	τ^0 (deg)	a_0	a_2	a_4	dihedral angle	τ^0 (deg)	a_0	a_2	a_4
$H_{10}O_9C_2C_3$	180.0	20.543 42	−23.060 90	2.517 47	$O_9C_2C_3C_4$	180.0	20.395 80	−23.060 90	2.665 10	$H_{13}C_5C_6C_7$	180.0	19.861 30	−23.060 90	3.199 60
$C_3C_4C_5C_6$	0.0	17.494 72	−23.060 90	5.566 17	$O_8C_1C_2C_3$	180.0	19.877 53	−23.060 90	3.183 37	$H_{14}C_6C_7C_1$	180.0	19.913 38	−23.060 90	3.147 52
$C_4C_5C_6C_7$	0.0	18.522 60	−23.060 90	4.538 30	$H_{11}C_3C_4C_5$	180.0	18.773 05	−23.060 90	4.287 85	$H_{15}C_7C_1C_2$	180.0	19.211 93	−23.060 90	3.848 97
$C_7C_1C_2C_3$	0.0	17.328 62	−23.060 90	5.732 28	$H_{12}C_4C_5C_6$	180.0	20.457 53	−23.060 90	2.603 37					

Bond−Bond Interaction Force Constants (kcal mol^{-1} Å^{-2})

bond i	bond j	$k_{ri,rj}$	bond i	bond j	$k_{ri,rj}$	bond i	bond j	$k_{ri,rj}$
C_1-C_2	$C_2=C_3$	106.169	$C_4=C_5$	C_5-C_6	22.703	$C_2=C_3$	C_2-O_9	43.898
$C_2=C_3$	C_3-C_4	32.689	C_5-C_6	$C_6=C_7$	87.819	C_1-C_2	$C_1=O_8$	36.310
C_3-C_4	$C_4=C_5$	113.367	$C_6=C_7$	C_1-C_7	101.602	C_1-C_7	$C_1=O_8$	65.390

Angle−Angle Interaction Force Constants (kcal mol^{-1} rad^{-2})

angle i	angle j	$k_{\theta i,\theta j}$	angle i	angle j	$k_{\theta i,\theta j}$	angle i	angle j	$k_{\theta i,\theta j}$
$H_{11}C_3C_4$	$C_3C_4H_{12}$	−12.141	$C_3C_4C_5$	$C_4C_5H_{13}$	26.574	$C_6C_7C_1$	$H_{14}C_6C_7$	8.895
$H_{13}C_5C_6$	$C_5C_6H_{14}$	−1.398	$C_4C_5C_6$	$H_{12}C_4C_5$	15.201	$H_{12}C_4C_5$	$C_4C_5H_{13}$	7.640
$C_1C_2C_3$	$C_2C_3H_{11}$	22.284	$C_5C_6C_7$	$C_6C_7H_{15}$	20.319	$H_{14}C_6C_7$	$C_6C_7H_{15}$	9.169

Bond−Angle Interaction Force Constants (kcal mol^{-1} Å^{-1} rad^{-1})

bond	angle	$k_{r,\theta}$	bond	angle	$k_{r,\theta}$	bond	angle	$k_{r,\theta}$
C_1-C_2	$O_8C_1C_2$	30.877	$C_4=C_5$	$C_4C_5C_6$	202.852	C_1-C_7	$H_{15}C_7C_1$	54.583
C_1-C_7	$C_7C_1O_8$	73.314	$C_6=C_7$	$C_5C_6C_7$	86.195	$C_2=C_3$	$C_2C_3H_{11}$	46.263
$C_1=O_8$	$C_7C_1O_8$	101.522	$C_6=C_7$	$C_6C_7C_1$	90.631	$C_4=C_5$	$H_{12}C_4C_5$	66.610
$C_1=O_8$	$O_8C_1C_2$	10.645	C_3-C_4	$H_{11}C_3C_4$	56.667	$C_4=C_5$	$C_4C_5H_{13}$	87.217
$C_2=C_3$	$C_1C_2C_3$	138.480	C_3-C_4	$C_3C_4H_{12}$	44.449	$C_6=C_7$	$H_{14}C_6C_7$	74.002
$C_2=C_3$	$C_2C_3C_4$	114.326	C_5-C_6	$H_{13}C_5C_6$	30.452	$C_6=C_7$	$C_6C_7H_{15}$	58.476
$C_4=C_5$	$C_3C_4C_5$	32.572	C_5-C_6	$C_5C_6H_{14}$	48.145			

Switching Function Parameters

$a = 3.5$ Å^{-1} $b = 0.28$ $c = 25.0$ Å^{-4}

[a] Atom numbers are defined in Figure 1.

is close to the barrier used by Smedarchina et al.[24] in calculations of the splittings in tropolone based on an instanton model. We note that a high barrier close to that obtained from SCF calculations was also used in our studies[2,4] of malonaldehyde (which has a similar structure to tropolone) and in the instanton treatment of malonaldehyde reported by Smedarchina et al.,[25] and the calculated splittings are in good agreement with experiments for the parent compound as well as several isotopomers. Moreover, Smedarchina et al.[24] considered several different levels of theory including AM1, MP2, and two density functional treatments in calculations of the barrier height for tropolone and found that all of the "higher" levels of theory predicted barriers that were entirely too low to yield a reasonable zero-point energy splitting.

B. Semiclassical Tunneling Model. Semiclassically, the action variables are the classical analogues of the quantum numbers. A wave function for a specified quantum state is represented by an ensemble of classical trajectories that lie on a KAM (Kolmogoroff−Arnold−Moser) invariant torus, with the action integrals quantized according to the EBK (Einstein−Brillouin−Keller) quantization condition,[26]

$$\int_{C_j} \mathbf{p}\, \mathrm{d}\mathbf{q} = 2\pi\hbar\left(n_j + \frac{\beta_j}{4}\right) \tag{5}$$

where C_j is a closed loop on the torus, n_j is the quantum number, and β_j is the Maslov index. For a symmetric double-well system, any torus corresponding to a given state on one side of the barrier has an equivalent (mirror image) torus on the other side. Tunneling between the tori can be treated with the Feynman path integral formalism.[27] In the path integral, the amplitude for a particle of energy E taking a particular path P on a potential V is proportional to $\exp(iS_P/\hbar)$, where S_P is the classical action along P. The total amplitude is the sum of these terms for all paths connecting the two end points. For tunneling processes the action S_P is imaginary, and thus the tunneling amplitude is exponentially damped. Hence, the amplitude sum is dominated by contributions from regions near the paths which minimize the action. These paths are trajectories in imaginary time which satisfy the classical equations of motion in the "upside-down" potential.[28] The crucial point in treating tunneling is to find these classical paths which connect the two tori associated with the specified quantum state. However, solving Hamilton's equations in the tunneling region is very difficult for multidimensional systems, and approximate approaches are often used instead.

Since the motion of the migrating hydrogen atom is faster than that of the other degrees of freedom, we will focus on the sudden approximation. Under this approximation, the wave functions can be separated as

$$\Psi_i(s,\mathbf{R}) = \chi_i(\mathbf{R})\, \Phi_i(s;\mathbf{R}) \tag{6}$$

where i denotes the left or right wells, s represents the tunneling coordinate, and $\mathbf{R}$ denotes the other degrees of freedom. In a simple quantum mechanical two-state problem, the energy level splitting is given by the matrix element

$$\begin{aligned}\Delta E &= 2\langle \Psi_{\mathrm{L}}(s,\mathbf{R})|H|\Psi_{\mathrm{R}}(s,\mathbf{R})\rangle \\ &= \langle \chi_{\mathrm{L}}(\mathbf{R})|\Delta E(\mathbf{R})|\chi_{\mathrm{R}}(\mathbf{R})\rangle\end{aligned} \tag{7}$$

where L and R denote the left and right wells, and

$$\Delta E(\mathbf{R}) = 2\langle \Phi_{\mathrm{L}}(s;\mathbf{R})|H|\Phi_{\mathrm{R}}(s;\mathbf{R})\rangle \tag{8}$$

TABLE 2: Calculated and ab Initio Normal-Mode Frequencies (cm^{-1}) for the Three Isotopomers of Tropolone Used in Parametrizing the Force Field

	parent compound				$^{13}C_1{}^{18}O_8{}^2H_{10}$				$^2H_{10}{}^2H_{12}{}^2H_{14-15}$			
mode	this work		ab initio		this work		ab initio		this work		ab initio	
7	106	A″	105	A″	104	A″	103	A″	101	A″	101	A″
8	174	A″	174	A″	171	A″	172	A″	167	A″	169	A″
9	353	A′	356	A′	341	A″	347	A″	331	A″	332	A″
10	354	A″	351	A″	347	A′	337	A′	347	A′	341	A′
11	376	A′	370	A′	360	A′	360	A′	362	A″	353	A″
12	386	A″	385	A″	379	A″	382	A″	369	A′	360	A′
13	445	A′	446	A′	440	A′	435	A′	437	A′	437	A′
14	536	A″	524	A″	518	A″	523	A″	494	A″	503	A″
15	546	A′	547	A′	532	A′	533	A′	531	A′	529	A′
16	639	A″	641	A″	598	A″	593	A″	582	A″	591	A″
17	710	A′	706	A′	648	A″	629	A″	609	A″	610	A″
18	733	A″	757	A″	703	A′	700	A′	660	A″	660	A″
19	761	A′	759	A′	748	A′	744	A′	681	A′	680	A′
20	786	A″	807	A″	775	A″	755	A″	708	A″	703	A″
21	849	A″	850	A″	843	A″	841	A″	743	A′	743	A′
22	913	A′	899	A′	902	A″	913	A″	759	A″	761	A″
23	920	A″	914	A″	909	A′	897	A′	800	A′	832	A′
24	952	A″	943	A″	935	A″	943	A″	864	A″	863	A″
25	985	A″	977	A″	961	A″	977	A″	870	A′	881	A′
26	988	A′	990	A′	985	A′	977	A′	915	A″	903	A″
27	1106	A′	1094	A′	1044	A′	1012	A′	935	A′	922	A′
28	1257	A′	1261	A′	1110	A′	1129	A′	992	A′	971	A′
29	1280	A′	1263	A′	1259	A′	1253	A′	1049	A′	1052	A′
30	1313	A′	1302	A′	1284	A′	1278	A′	1121	A′	1140	A′
31	1351	A′	1344	A′	1305	A′	1305	A′	1192	A′	1185	A′
32	1416	A′	1379	A′	1360	A′	1371	A′	1332	A′	1324	A′
33	1467	A′	1474	A′	1422	A′	1450	A′	1363	A′	1365	A′
34	1485	A′	1497	A′	1481	A′	1474	A′	1452	A′	1450	A′
35	1552	A′	1552	A′	1514	A′	1527	A′	1532	A′	1516	A′
36	1593	A′	1597	A′	1587	A′	1585	A′	1588	A′	1587	A′
37	1635	A′	1641	A′	1611	A′	1603	A′	1615	A′	1606	A′
38	1672	A′	1677	A′	1665	A′	1672	A′	1654	A′	1660	A′
39	1710	A′	1717	A′	1686	A′	1695	A′	1696	A′	1699	A′
40	3217	A′	3232	A′	2494	A′	2496	A′	2400	A′	2385	A′
41	3245	A′	3240	A′	3217	A′	3232	A′	2409	A′	2397	A′
42	3246	A′	3257	A′	3245	A′	3240	A′	2417	A′	2410	A′
43	3251	A′	3260	A′	3246	A′	3257	A′	2494	A′	2496	A′
44	3264	A′	3266	A′	3251	A′	3260	A′	3246	A′	3256	A′
45	3426	A′	3432	A′	3264	A′	3266	A′	3264	A′	3258	A′

is the tunneling splitting in the s direction for a fixed value of **R**. Thus, the total energy level splitting can be obtained by calculating the one-dimensional splitting $\Delta E(\mathbf{R})$ in the s direction for every parametric value of **R** and then averaging over **R**. In a quasiclassical trajectory simulation, this averaging is performed by using an ensemble of trajectories with random initial vibrational phases. Within the framework of the WKB approximation, the semiclassical expression for the energy splitting in a one-dimensional symmetric double well is given by[29]

$$\Delta E = 2\hbar\nu \exp(-\theta) \tag{9}$$

where ν is the frequency of the oscillator at total energy E_0 and θ is the usual WKB barrier penetration integral

$$\theta = \frac{1}{\hbar} Im \int p_s \, ds = \frac{1}{\hbar} \int_{s<}^{s>} [2m[V(s) - E_0]]^{1/2} \, ds \tag{10}$$

The limits of the integral are the classical turning points on the two sides of the barrier, corresponding to energy $E = E_0$.

A semiclassical method that incorporates the preceding into classical trajectory simulations can be formulated as follows. A trajectory is initiated in one of the wells and propagated in the classically allowed region of phase space. Each time a turning point occurs, i.e., the component of the momentum of the tunneling particle along the s direction is zero, an amplitude factor $e^{-\theta}$ is computed with all of the other degrees of freedom frozen. The tunneling splitting is given by[30]

$$\Delta E = 2\hbar \frac{d}{dt} \langle S(t) \rangle \tag{11}$$

where $S(t)$ is the accumulated amplitude factor

$$S(t) = \sum h(t - t_n) e^{-\theta_n} \tag{12}$$

Here, t_n are the times that a trajectory is at turning points along s, and $h(x)$ is the usual step function which is 1 if $x > 0$ and 0 if $x < 0$. The bracket implies an ensemble average over the initial vibrational phases. Typical plots of $\langle S(t) \rangle$, from which the splitting is derived by way of eq 11 are shown in Figure 2 for the ground states of the normal (panel a) and deuterated (panel b) species. The reader should note that, up to this point, the approach we have described is equivalent to that presented by Makri and Miller.[30]

It should be emphasized that $\langle S(t) \rangle$ is not the total tunneling amplitude as a function of time; that is, the semiclassical method is not an analogue of a time-dependent quantum mechanical calculation in which a state initially localized in one of the wells is propagated and the probability amplitude of the system being in the other well is computed as a function of time. Calculating $\langle S(t) \rangle$ is merely a way to obtain the level splitting given by eq 7.

TABLE 3: Comparison of Calculated and ab Initio Normal-Mode Frequencies (cm^{-1}) for Two Isotopomers of Tropolone Not Used in Parametrizing the Force Field

	$^2H_{10}$				$^{18}O_8$			
mode	this work		ab initio		this work		ab initio	
7	105	A″	105	A″	105	A″	103	A″
8	174	A″	172	A″	172	A″	174	A″
9	348	A″	351	A″	350	A′	351	A′
10	349	A′	343	A′	352	A″	350	A″
11	370	A′	365	A′	366	A′	366	A′
12	383	A″	384	A″	385	A″	385	A″
13	442	A′	440	A′	444	A′	442	A′
14	519	A″	523	A″	535	A′	538	A′
15	544	A′	544	A′	535	A″	524	A″
16	599	A″	594	A″	639	A″	640	A″
17	649	A″	641	A″	709	A′	703	A′
18	706	A′	705	A′	733	A″	757	A″
19	761	A′	755	A′	749	A′	750	A′
20	775	A″	758	A″	786	A″	807	A″
21	843	A″	842	A″	849	A″	850	A″
22	905	A″	914	A″	912	A′	899	A′
23	910	A′	899	A′	920	A″	914	A″
24	935	A″	943	A″	952	A″	943	A″
25	962	A″	977	A″	985	A″	977	A″
26	987	A′	978	A′	988	A′	989	A′
27	1045	A′	1014	A′	1106	A′	1093	A′
28	1111	A′	1133	A′	1257	A′	1261	A′
29	1259	A′	1262	A′	1280	A′	1262	A′
30	1286	A′	1278	A′	1312	A′	1302	A′
31	1317	A′	1312	A′	1350	A′	1343	A′
32	1365	A′	1372	A′	1413	A′	1379	A′
33	1432	A′	1457	A′	1466	A′	1471	A′
34	1482	A′	1486	A′	1484	A′	1497	A′
35	1551	A′	1546	A′	1540	A′	1546	A′
36	1593	A′	1595	A′	1593	A′	1592	A′
37	1631	A′	1630	A′	1627	A′	1633	A′
38	1670	A′	1674	A′	1671	A′	1677	A′
39	1701	A′	1710	A′	1710	A′	1710	A′
40	2494	A′	2496	A′	3217	A′	3232	A′
41	3217	A′	3232	A′	3245	A′	3240	A′
42	3245	A′	3240	A′	3246	A′	3257	A′
43	3246	A′	3257	A′	3251	A′	3260	A′
44	3251	A′	3260	A′	3264	A′	3266	A′
45	3264	A′	3266	A′	3426	A′	3432	A′

It is important to appreciate this to properly determine the action integral. Note that the two wave functions $\Psi_L(s,\mathbf{R})$ and $\Psi_R(s,\mathbf{R})$ in eq 7 are associated with two identical tori that are mirror images of each other. Thus, the tunneling path connecting the two tori should be symmetric in the *full-dimensional* space, which means that the positions of all the atoms have to be symmetrically reflected as the H-atom goes from one well to another during calculation of the action integral. This cannot be accomplished for many-atom systems by using a strict sudden approximation such as that proposed by Makri and Miller,[30] because the barrier to the H-atom motion would not be symmetric except at the transition state if all the degrees of freedom except the tunneling one(s) were held fixed during the tunneling process. This is illustrated in Figure 3. Frame a of Figure 3 depicts the actual potential along the tunneling direction with all of the other degrees of freedom frozen. Since the motion is followed classically in only one well, a typical barrier to the hydrogen atom transfer will not reflect the mirror image configuration of the molecule; i.e., the potential will not be symmetric along the tunneling coordinate. Thus, in the calculation of the action integrals, we employ the sudden approximation to obtain the potential in only the reactant well and then assume it is symmetric on the other side. In other words, the tunneling probability is determined by assuming a symmetric potential, as illustrated in Figure 3b.

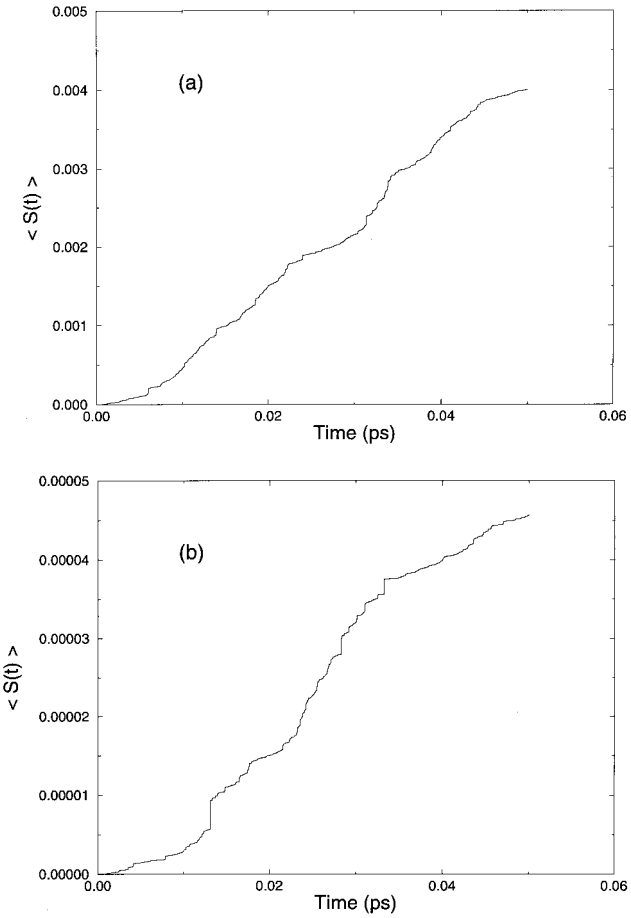

Figure 2. Plots of tunneling amplitude factor versus time. Results are for the ground states of the normal (panel a) and deuterated (panel b; the migrating hydrogen is substituted with deuterium) species.

We evaluate the action integral from the inner turning point $s_<$ to the point s_{sym} that lies in the plane separating the two wells, and then multiply the result by 2:

$$\theta = \frac{2}{\hbar} Im \int_{s_<}^{s_{sym}} p_s \, ds \tag{13}$$

The point s_{sym} corresponds to $r_{OH} = r_{O\cdots H}$. The conjugate momentum p_s in eq 13 can be obtained by using energy conservation along the tunneling path

$$\frac{p_s^2}{2m} + \frac{\mathbf{P}_R^2}{2\mu} + V(s,\mathbf{R}) = \frac{p_s^2(t_n)}{2m} + \frac{\mathbf{P}_R^2(t_n)}{2\mu} + V(s,\mathbf{R})|_{t_n} \tag{14}$$

where t_n is the time that a trajectory is at turning point n. Under the sudden approximation, $\mathbf{R}$ and $\mathbf{P}_R$ are held fixed during calculation of the action integral. Moreover, $p_s(t_n) = 0$ at a turning point. Hence, the action integral can be written as

$$\theta = \frac{2}{\hbar} Im \int_{s_<}^{s_{sym}} p_s \, ds = \frac{2}{\hbar} \int_{s_<}^{s_{sym}} [2m\{V(s,\mathbf{R}) - V(s,\mathbf{R})|_{t_n}\}]^{1/2} \, ds \tag{15}$$

One of the central issues of the method is the specification of the tunneling path s. In the sudden limit, the tunneling path is a straight line through the barrier separating the two wells. Thus, we have chosen straight-line paths parallel to the equilibrium O−O distance vector. We have also investigated other paths that deviate somewhat from straight lines. The results discussed below indicate that the straight-line paths are the best choice for this system.

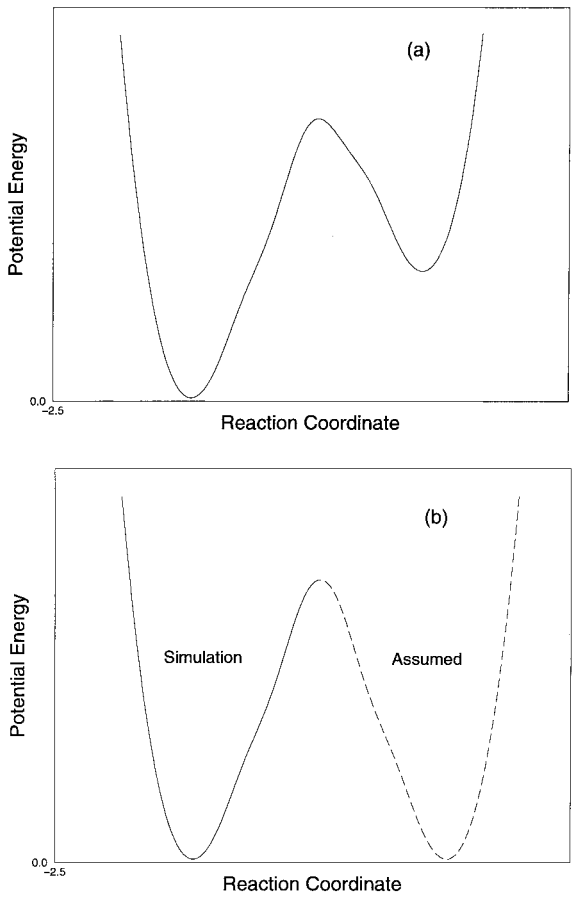

Figure 3. Illustration of the potential energy along the reaction coordinate. (a) The potential is asymmetric if a strict sudden approximation is used. (b) In calculation of the tunneling integral, the sudden approximation is employed to obtain the potential up to the midpoint and then assumed to be symmetric on the other side.

C. Details of Trajectory Calculations. To rigorously describe semiclassical tunneling from a given quantum state, one should choose the classical trajectories that lie on the invariant torus corresponding to the quantum state of interest. This could be accomplished in principle by using adiabatic switching,[31] where a time-dependent Hamiltonian is used to slowly transform the Hamiltonian from a simple zero-order form to the actual one of interest. This is, however, a nontrivial task for a complicated multidimensional system. We instead use quasiclassical normal-mode sampling.[32] Initial conditions were chosen from the quantum torus of the zero-order (harmonic) Hamiltonian with the action angles randomly selected in the interval $(0,2\pi)$, after which the coordinates and momenta were scaled to give the desired total energy. Although this method gives mode-selective rather than state-selective initial conditions, it is probably good enough for the low energies considered here.

Ensembles of 2500 classical trajectories were used for each set of initial conditions. The angular momentum was zero in all calculations. The trajectories were integrated in a lab fixed Cartesian coordinate system by using a fourth-order Runge−Kutta−Gill integrator with a fixed stepsize of 3×10^{-17} s. The length of the individual trajectories was 0.05 ps, and there were about four turning points observed for each trajectory. The short run time was used to ensure that the initial state remains almost unchanged, since the eigenvalue splitting is associated with time-independent eigenstates of the Hamiltonian. It is well-known that the classical trajectory method is often inaccurate for describing long-time dynamics of polyatomic systems. Thus, we have used a short run time (0.05 ps, which is about 2 orders of magnitude smaller than that usually used in reaction dynamics studies) so that the trajectory simulations approximate stationary eigenstates, and the problems associated with long classical trajectories (such as the aphysical flow of the zero-point energy[32]) should not be significant.

TABLE 4: Calculated Tunneling Splittings for the $\tilde{X}$ State and the Measured Splittings for the $\tilde{A}$ State

vibrational mode	obsd freq[a] (cm^{-1})		splittings[b] (cm^{-1})	
	$\tilde{X}$ state	$\tilde{A}$ state	expt[c]	this work
ground state (H)	$\tilde{X}$		0.97	0.97
ground state (D)	$\tilde{X}$		0.0	0.01
ground state (H)		$\tilde{A}$	20	
ground state (D)		$\tilde{A}$	2	
7	110	39	11 (8)	0.83 (0.77)
8	177	171	8 (5)	0.90 (0.74)
9	349			1.3
10	271	269	(10)	0.98 (1.0)
11	359	296	31	2.7
12	335			0.88
13	434	414	33	1.2
14	676			0.87
15	551			1.1
16	720			1.0
17	751			0.98
18	674	640	18	1.3
19	741	511	14	1.0
20	774			1.1
21	828			1.1
22	908			1.0
23	875			1.0
24	983			1.1
25	1000			1.4
26	989			1.0
27	1146			1.1
28	1252			1.2
29	1274			1.2
30	1412			1.2
31	1427			1.1
32	1460			2.2
33	1470			2.6
34	1481			1.5
35	1499			1.3
36	1522			1.0
37	1565			1.3
38	1628			1.2
39	1635			1.1
40	3006			1.0
41	3023			0.97
42	3030			0.91
43	3055			0.95
44	3055			0.94
45	3121			31.1

[a] Taken from Takada and Nakamura.[23] [b] Numbers given in parentheses are the splittings for the second vibrationally excited states. [c] Taken from Takada and Nakamura[23] and Smedarchina et al.[24]

3. Results and Discussion

The main motivation of this study was to further illustrate and test the semiclassical method we have been using for treating tunneling. We calculated the level splittings for the ground states of the normal and deuterated forms of tropolone. We also studied the sensitivity of the splitting to the choice of the tunneling path. Finally, we did a series of calculations for initial conditions corresponding to mode-selective excitations to investigate the effects of vibrational excitations on tunneling.

A. Vibrational Ground State. The calculated splittings for the ground states of the normal and deuterated (the migrating hydrogen is substituted with deuterium) species are given in the first row of Table 4, along with the corresponding

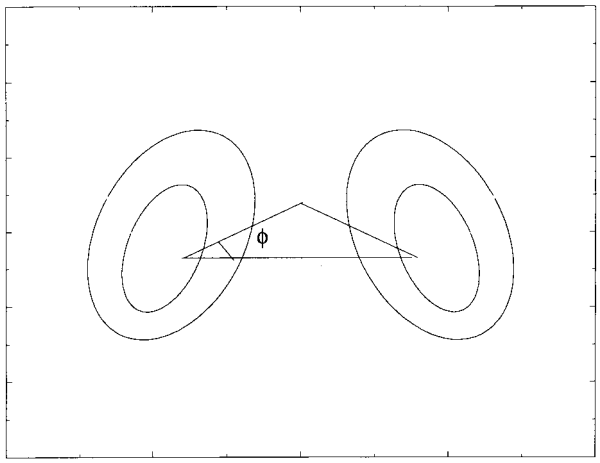

Figure 4. Illustration of the tunneling paths used in this study.

TABLE 5: Computed Ground-State Splitting for Different Tunneling Paths[a]

ϕ (deg)	tunneling splitting (cm^{-1})	ϕ (deg)	tunneling splitting (cm^{-1})
−15	0.84	0	0.96
−10	0.92	5	0.92
−5	0.96	10	0.84
−2	0.96	15	0.73

[a] The case of $\phi = 0$ corresponds to straight-line paths.

experimental results. It should be noted again that since the barrier height is not accurately known for this system, the splitting for the ground state of the normal species was obtained by adjusting the barrier height to obtain agreement with the measured splitting. The agreement between the experimental and calculated splittings for the deuterated species indicates that the barrier height (16.0 kcal/mol) thus determined is probably reasonable. This value is close to that (15.7 kcal/mol) predicted by using the HF/6-31G** basis set. A barrier height close to the one obtained at the Hartree−Fock level was also used in our earlier study of malonaldehyde[4] (which is structurally similar to tropolone), and the calculated splittings are in good accord with experiments. This suggests that an accurate treatment of tunneling can provide direct, quantitative information about the barrier.

To check the precision of our calculations, we computed the ground-state splitting for four independent trajectory ensembles. The results are 0.94, 0.96, 0.97, and 1.00 cm^{-1}. The average reported in Table 4 is 0.97 cm^{-1}, and the standard deviation is 0.025 cm^{-1}. Thus, statistical errors in the calculations are not significant.

The results given in Table 4 were obtained by using straight-line paths parallel to the O−O direction in the equilibrium structure. Other paths, chosen to be two-piece straight lines that are symmetric with respect to the plane separating the two wells (see Figure 4), were also tested. These paths and straight lines along the equilibrium O−O direction form isosceles triangles. The calculated splittings are given in Table 5. Here ϕ is the angle between the equilibrium O−O distance vector and the specified tunneling direction. The $\phi = 0$ case is one of the four ensembles used in the calculation of the ground-state splitting. The same ensemble of classical trajectories was used in the calculations for all of the other values of ϕ to ensure that the statistical errors have no qualitative effect. The tunneling integral was computed each time the component of the momentum of the migrating hydrogen atom along the tunneling direction (defined by ϕ) became zero. It is clear from Table 5 that the simple straight-line paths yield the largest splitting (smallest action). However, the computed splitting is not very sensitive to variations in path, which is reasonable since it is a result averaged over multidimensional space.

B. Vibrationally Excited States. The tunneling splittings of several vibrationally excited states have been measured for the first electronically excited state $\tilde{A}^1\ B_2$.[15−19] The most interesting finding is that some modes promote tunneling, some suppress it, and some do not affect it. This clearly demonstrates the effects of multidimensional dynamics on the tunneling process and the importance of properly treating the motions of skeletal atoms.

To investigate the effects of vibrational excitation on tunneling, we calculated the tunneling splittings for the X state with initial conditions where each normal mode was first assigned zero-point energy and then a selected normal mode was assigned an additional one or two quanta of energy. This was done for each of the 39 normal modes. The results are given in Table 4, together with the available experimental data for the $\tilde{A}$ state.

Comparing the respective ground-state splittings with the computed and observed splittings in the low-frequency regime where the experimental data are available, it appears that many of the modes that significantly enhance (or suppress) the ground-state tunneling are similar for the X and $\tilde{A}$ states. That is, although one cannot compare directly the tunneling splittings for analogous mode-specific excitations on the X and $\tilde{A}$ states (they differ by approximately an order of magnitude), there is a fairly good correlation between the relative effects of selective excitation of mode "*i*" on the calculated splittings in the ground state and the corresponding effects of that same mode on the splitting measured for the first electronic excited state. This suggests that many of the data for the $\tilde{A}$ state of tropolone may be qualitatively interpreted from the theoretical calculations for the X state.

It is obvious (see Tables 2 and 4) that all the normal modes which, when excited, give rise to smaller splittings than that of the ground state are out-of-plane modes. The fact that out-of-plane motions suppress tunneling was also observed for malonaldehyde.[4] The most plausible explanation for this is that the out-of-plane motions tend to increase the effective height and width of the barrier to tunneling. For example, excitation of the lowest frequency mode (105 cm^{-1}), which yields the largest out-of-plane "scissoring" motion of the two oxygen atoms, results in a reduced splitting (0.83 cm^{-1}). This was explicitly discussed in ref 4.

The highest splitting (31.2 cm^{-1}) results from excitation of the O−H stretching mode (mode 45). This is not surprising since the excitation of O−H assigns energy directly to the tunneling coordinate. Relatively large splittings are also observed for excitations of modes 11 (O−O in-plane motion), 32 (HOC bend), and 33 (O−H stretch, O═C_1−C_2 bend).

In general, excitation of modes that involve motions of the migrating H atom or the two oxygens have significant effects on tunneling. Whether tunneling is suppressed or enhanced depends on the character of the excited mode. Excitations of the modes that are due mainly to C−H stretching (modes 40−44) have negligible effect on the splitting. Intermediate effects on the splittings are obtained for excitations of most of the other modes.

4. Conclusions

We have investigated tunneling effects in tropolone by using a semiclassical method that we have described previously.[4] Since

the method includes tunneling calculations in standard trajectory simulations, we are able to explicitly treat all 39 vibrational degrees of freedom and thus investigate the effects of multidimensional classical dynamics on hydrogen-atom tunneling in this large polyatomic molecule.

The potential-energy surface is largely based on ab initio information. The barrier to classical isomerization on the potential-energy surface is 16.0 kcal/mol, a value close to that obtained from HF/6-31G** calculations. This barrier was obtained by fitting the calculated ground-state splitting in the normal species to the experimental value. Using this barrier, the calculated ground-state splitting in the deuterated species is in good accord with experiment. This suggests that the treatment of tunneling may be useful for determining barriers.

We have also examined alternative tunneling paths. They were chosen to be two-piece straight lines that are symmetric with respect to the plane separating the two wells (see Figure 4). These paths and straight lines along the equilibrium O−O direction form isosceles triangles. We found that simple straight-line paths yield the largest splitting. However, the computed splitting is not very sensitive to variations in path, which is reasonable because the splitting is a result averaged over multidimensional space.

The effects of vibrational excitations on the tunneling were investigated by performing a series of calculations for initial conditions corresponding to mode-selective excitations. Although the calculations were carried out for the ground electronic state (X) while all of the measured splittings of the vibrationally excited states are for the first electronically excited state ($\tilde{A}$), comparisons of the calculated and observed splittings indicate that many of the modes that significantly affect tunneling are similar for the X and $\tilde{A}$ states. Thus, many of the data for the $\tilde{A}$ state may be qualitatively interpreted from calculations for the X state. We found that excitations of certain out-of-plane modes suppress tunneling; in-plane modes that involve the motions of the migrating H atom and the two oxygen atoms (O−H stretch, HOC bend, and O═C_1−C_2 bend) significantly enhance tunneling; and excitations of the rest of the modes have negligible or limited effect on tunneling.

Acknowledgment. Y.G. and D.L.T. are supported by the U. S. Army Research Office. T.D.S. is supported by the United States Department of Energy.

References and Notes

(1) Sewell, T. D.; Thompson, D. L. *Chem. Phys. Lett.* **1992**, *193*, 347.

(2) Guo, Y.; Sewell, T. D.; Thompson, D. L. *Chem. Phys. Lett.* **1994**, *224*, 470.

(3) Qin, Y.; Thompson, D. L. *J. Chem. Phys.* **1994**, *100*, 6445.

(4) Sewell, T. D.; Guo, Y.; Thompson, D. L. *J. Chem. Phys.* **1995**, *103*, 8557.

(5) Guo, Y.; Qin, Y.; Sorescu, D. C.; Thompson, D. L. *J. Chem. Phys.* **1996**, *104*, 4041.

(6) Guo, Y.; Thompson, D. L. *J. Chem. Phys.* **1996**, *105*, 1070.

(7) Guo, Y.; Thompson, D. L. *J. Chem. Phys.* **1996**, *105*, 7480.

(8) George, T. F.; Miller, W. H. *J. Chem. Phys.* **1972**, *56*, 5722; **1972**, *57*, 2458.

(9) Chapman, S.; Garrett, B. C.; Miller, W. H. *J. Chem. Phys.* **1975**, *63*, 2710.

(10) Alves, A. C. P.; Hollas, J. M. *Mol. Phys.* **1972**, *23*, 927; **1973**, *25*, 1305.

(11) Redington, R. L.; Redington, T. E. *J. Mol. Spectrosc.* **1979**, *78*, 229.

(12) Rossetti, R.; Brus, L. E. *J. Chem. Phys.* **1980**, *73*, 1546.

(13) Sekiya, H.; Nagashima, Y.; Nishimura, Y. *Chem. Phys. Lett.* **1981**, *160*, 581.

(14) Tomoika, Y.; Ito, M.; Mikami, N. *J. Phys. Chem.* **1983**, *87*, 4401.

(15) Alves, A. C. P.; Hollas, J. M.; Musa, H.; Ridley, T. *J. Mol. Spectrosc.* **1985**, *109*, 99.

(16) Redington, R. L.; Chen, Y.; Scherer, G. J.; Field, R. W. *J. Chem. Phys.* **1988**, *88*, 627.

(17) Sekiya, H.; Nagashima, Y.; Nishimura, Y. *J. Chem. Phys.* **1990**, *92*, 5761.

(18) Redington, R. L.; Redington, T. E.; Hunter, M. A.; Field, R. W. *J. Chem. Phys.* **1990**, *92*, 6456.

(19) Sekiya, H.; Nagashima, Y.; Tsuji, T.; Nishimura, Mori, Y. A. *J. Phys. Chem.* **1991**, *95*, 10311.

(20) Redington, R. L. *J. Chem. Phys.* **1990**, *92*, 6447.

(21) Redington, R. L.; Bock, C. W. *J. Phys. Chem.* **1991**, *95*, 10284.

(22) Vener, M. V.; Scheiner, S.; Sokolov, N. D. *J. Chem. Phys.* **1994**, *101*, 9755.

(23) Takada, S.; Nakamura, H. *J. Chem. Phys.* **1995**, *102*, 3977.

(24) Smedarchina, Z.; Siebrand, W.; Zgierski, M. Z. *J. Chem. Phys.* **1996**, *104*, 1203.

(25) Smedarchina, Z.; Siebrand, W.; Zgierski, M. Z. *J. Chem. Phys.* **1995**, *103*, 5326.

(26) Gutzwiller, M. C. *Chaos in Classical and Quantum Mechanics;* Springer-Verlag: New York, 1990.

(27) Feynman, R. P.; Hibbs, A. R. *Quantum Mechanics and Path Integrals;* McGraw-Hill: New York, 1965.

(28) Miller, W. H. *J. Chem. Phys.* **1975**, *62*, 1899.

(29) Miller, W. H. *J. Phys. Chem.* **1979**, *83*, 960.

(30) Makri, N.; Miller, W. H. *J. Chem. Phys.* **1989**, *91*, 4026.

(31) Johnson, B. R. *J. Chem. Phys.* **1984**, *83*, 1204.

(32) Raff, L. M.; Thompson, D. L. In *Theory of Chemical Reaction Dynamics*; Baer, M., Ed.; Chemical Rubber Co.: Boca Raton, FL, 1985).

(33) Guo, Y.; Sewell, T. D.; Thompson, D. L. *J. Chem. Phys.* **1996**, *104*, 576.